International Journal of Mechanical And Production Engineering, ISSN: 2320-2092, Volume- 5, Issue-7, Jul.-2017
http://iraj.in

HRTEM AND MC SIMULATION STUDY OF NC-TIN/A-(C,CN_X) NANOCOMPOSITE FILMS

A. NAWAZ, Y.G. SHEN

Department of Mechanical & Biomedical Engineering, City University of Hong Kong, Hong Kong, China
E-mail: meshen@cityu.edu.hk

Abstract- The grain growth in two-phase nanocomposite Ti-C_x-N_y thin films grown by reactive close-field unbalanced magnetron sputtering in an Ar-N_2 gas mixture with microstructures comprising of nanocrystalline (nc-) Ti(N,C) phase surrounded by amorphous (a-) (C,CN_x) phase was investigated by a combination of high-resolution transmission electron microscopy (HRTEM) and Monte Carlo (MC) simulations. The HRTEM results revealed that amorphous-free solid solution Ti(C,N) thin films exhibited polycrystallites with different sizes, orientations and irregular shapes. The grain size varied in the range between several nanometers and several decade nanometers. Further increase of C content (up to ~19 at.% C) made the amorphous phase wet nanocrystallites, which strongly hindered the growth of nanocrystallites. As a result, more regular Ti(C,N) nanocrystallites with an average size of ~5 nm were found to be separated by ~0.5-nm amorphous phases. When C content was further increased (up to ~48 at.% in this study), thicker amorphous matrices were produced and followed by the formation of smaller sized grains with lognormal distribution. Our MC analysis indicated that with increasing amorphous volume fraction (i.e. increasing C content), the transformation from nc/nc grain boundary (GB)-curvature-driven growth to a/nc GB-curvature-driven growth is directly responsible for the observed grain growth from great inhomogeneity to homogeneity process.

Keywords- Film Deposition; Composite Materials; Monte Carlo Methods; Structure; Transmission Electron Microscopy

I. INTRODUCTION

The possibility of growing two- or three-phase nanocomposite thin films with microstructures comprising of nanocrystalline phase in amorphous matrix has been reported recently [1,2]. For example, nanocrystalline (nc-) TiN/amorphous (a-) C-CN_x composite films were successfully synthesized by reactive magnetron sputtering [3,4]. By adding small amounts of carbon into a growing TiN film, a diffusive barrier was created to block dislocations and the plastic deformation was significantly suppressed, thus improving the mechanical properties of nc-TiN/a-(C,CN_x). Moreover, an increase in hardness coincides with a decrease in grain size due to the strong grain refinement, revealing a high density of grain boundaries. However, details of the interaction of the embedded solid solution (SS) nc-Ti(N,C) with a-(C,CN_x) matrices are not well known.

In this study, nanocomposite nc-TiN/a-(C,CN_x) films were produced by reactive magnetron sputtering. The atomic concentration of elements and their phase bonding were characterized by x-ray photoelectron spectroscopy (XPS). Microstructure of the films was revealed by high-resolution transmission electron microscopy (HRTEM) and x-ray diffraction (XRD). A Monte Carlo (MC) simulation based on the Potts model has also been developed to model how a-C or a-(C,CN_x) matrix influences the TiN crystal grain growth.

II. EXPERIMENTAL

Nanocomposite nc-TiN/a-(C,CN_x) films were deposited at 500 ºC in a reactive unbalanced dc magnetron sputtering system (UDP450, Teer Coating Limited) using two Ti and two C targets. The substrates used in this work were commercially available single crystal Si(100) wafers. The substrates were taken directly from sealed containers and introduced into the deposition chamber without further cleaning treatment. The sputtering was carried out in an Ar-N_2 gas mixture with a substrate rotation speed of 15 rpm. The base pressure in the chamber was $\leq 2.7\times10^{-4}$ Pa, and the working pressure, consisting of Ar and N_2 with a constant gas-flow rate of $F(N_2)+F(Ar)=40$ sccm, was set at 0.26×10^{-2} Pa during all depositions. All films were deposited to a nominal thickness of approximately 2.0 μm at a pulsed bias voltage of –60 V and a frequency of 250 kHz (~500 nm pulse width).

The atomic concentration of elements as well as their phase bonding were analyzed by XPS on a PHI 5802 system with a monochromatic Al K_α X-ray source ($h\nu$=1486.6 eV). The structure of the films was analyzed by XRD (Simens D500) in θ-2θ configuration. The HRTEM images were obtained in a JEOL JEM-2010F field emission electron microscope operated at 200 kV.

III. MONTE CARLO SIMULATION

MC simulation is performed on a two-dimensional (2D) N×N triangular lattice. Crystal species A and amorphous species B are assumed to occupy the lattice sites with periodic boundary conditions [5]. The energy change associated with each event can be calculated from the system Hamiltonian. Three energy contributions are considered: interfacial energy between species A and B, grain boundary

energy of species A, and surface energy of both A and B. Thus, in normal grain growth the Hamiltonian H can be written as:

$$H = \frac{1}{2} J_{AB} \sum_{i=1}^{N^2} \sum_{j=1}^{NN} (1 - \delta_{S_i S_j}) + \frac{1}{2} J_{AA} \sum_{i=1}^{N^2} \sum_{j=1}^{NN_C} (1 - \delta_{Q_i Q_j}) + N_A \times E_A + (N^2 - N_A) \times E_B \quad (1)$$

where NN is the nearest neighbors of a lattice site with N_A occupied by species A. J_{AA} and J_{AB} scale the grain boundary energy of species A and the interfacial energy between species A and B, respectively. E_A and E_B scale the surface energy of species A and B. $\delta_{S_i S_j}$ or $\delta_{Q_i Q_j}$ is Kronecker delta function. Two processes of lattice site re-orientation and site exchange are considered to realize the GB sliding by using standard MC techniques [6,7]. According to the condition that J_{AA} and J_{AB} required to form continuous amorphous matrix with enough V_a [7], we set J_{AB}=1 k_BT and J_{AA}=3 k_BT to determine the effects of V_a on grain growth. V_a varies from 1.5% to 45% and MC steps equal to 500 and 1500, respectively. After a simulation with a given V_a and MC steps finishing, the microstructure, grain diameter D_i and its total number N_i are recorded.

IV. RESULTS AND DISCUSSION

Figure 1(a) is a typical HRTEM image of thin film incorporating 7.3 at.% C ($TiC_{0.14}N_{0.74}$). It is found that the $TiC_{0.14}N_{0.74}$ still exhibits polycrystallite comprising of smaller grains in various sizes, shapes and orientations. Among the four grains, grain A shows cross {111} lattice fringe contrast with a lattice space of ~2.4 Å, while single {111} and {200} lattice fringe contrasts with lattice spaces of ~2.4 and ~2.1 Å respectively are observed in grains B~D respectively. The FFT spectrum in the insert shows some fluctuant, which indicates that there is a slight difference in lattice space in different parts of one grain or different grains due to the formation of SS Ti(N,C), resulting from the dissolution of C into TiN lattice. The SAD ring pattern in the insert can also be indexed in terms of an fcc structure, which is the same as that of pure TiN [see the inset of Fig. 2(a)]. When C content was increased to 19.1 at.% ($TiC_{0.39}N_{0.66}$), a distinguished change took place in the HRTEM image, as shown in Fig. 1(b). The nano-grains such as A~G with an average size of ~5 nm in diameter are found to be surrounded by ~0.5 nm thick amorphous phase, which consists of mainly sp^2 disordered carbon, graphite and minor CN_x according to Raman vibration and XPS bonding analysis (not shown here). It is interesting to note that ~0.5 nm thick amorphous phase wets all nanocrystallites. The grain shape becomes more regular because of hindrance of amorphous phase. The FFT spectrum in the insert shows some fluctuant spots along {111} and {200} rings, which indicates that there is a slight difference in lattice space for different grains due to the formation of SS Ti(N,C), resulting from the dissolution of C into TiN lattice. The {111} lattice fringes with a lattice space of ~0.25 nm are found in the most nanocrystallites such as A~D, while {200} lattice fringes with a lattice space of ~0.21nm are occasionally found in the nano-grains such as E. They are consistent with the inserted SAD pattern, which contains strong (200), (220) and weak (111) rings.

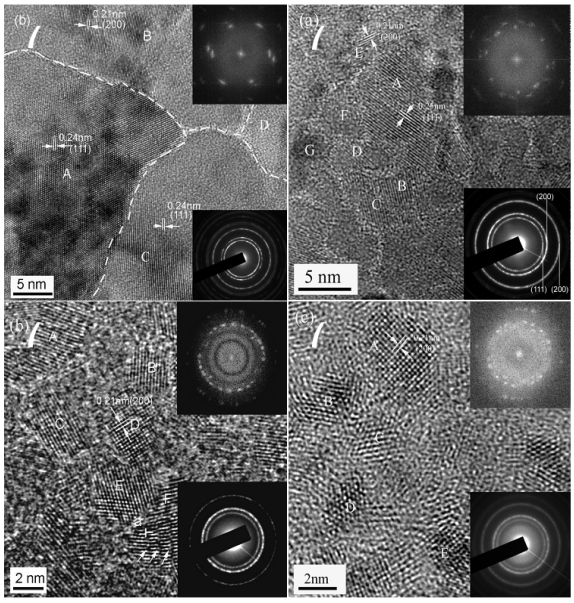

FIGURE 1. Plan-view HRTEM images obtained from four nanocomposite thin films with different C contents. (a) 7.3 at.% ($TiC_{0.14}N_{0.74}$), (b) 19.1 at.% ($TiC_{0.39}N_{0.66}$), (c) 33.2 at.% ($TiC_{0.81}N_{0.63}$) and (d) 48.2 at.% ($TiC_{1.61}N_{0.73}$) carbon. Their FFT spectra and corresponding SAD patterns are inserted respectively.

A HRTEM image obtained from $TiC_{0.81}N_{0.63}$ after incorporating more C (33.2 at.%) is shown in Fig. 1(c). It is found that nanocrystallites are separated by more amorphous matrices with an average thickness of ~3 nm, while their sizes are reduced to ~ 2-4 nm in diameter. Just similar with that in Fig. 1(b), the FFT spectrum in the insert shows some fluctuant spots along {200} ring, which results from dissolution of C into nanocrystallites. Besides, the {200} Bragg reflection in the SAD pattern looks stronger compared with that of $TiC_{0.39}N_{0.66}$ [see Fig. 1(b)], which was activated by enhanced preferred [200] orientation. Thus more C incorporation not only reduced grain size [also proved by XRD measurement in Fig. 2(a)], but also promoted formation of more (200) oriented nanocrystallites. When the carbon content was further increased to 48.2 at.% ($TiC_{1.61}N_{0.73}$), the density of nanocrystalline grains embedded into amorphous matrices was greatly decreased, accompanying with a further decrease of grain size to 1-2 nm, as shown in Fig. 1(d). It is consistent with an obvious diffused halo in the SAD pattern. In Fig. 1(d), almost nanocrystallites such as A~E possess (200) lattice fringes of ~0.21 nm, which is consistent with its FFT

spectrum in the insert. The structure of grain D relaxes due to its small grain size.

The decrease in the average TiN grain size with increasing C content in nc-TiN/a-(C,CN_x) films is shown in Fig. 2(a). The value of the mean grain size was obtained by averaging the grain size values calculated from XRD (111) and (200) diffraction peaks using the full width at half maximum (FWHM) value of the corresponding XRD peaks and the Scherrer equation [9]. The crystalline film for the pure TiN had a grain size of ~32 nm, whereas at C content of 19.0 at.% the grin size was smaller (~10 nm), in good agreement with the HRTEM observations (see Fig. 1).

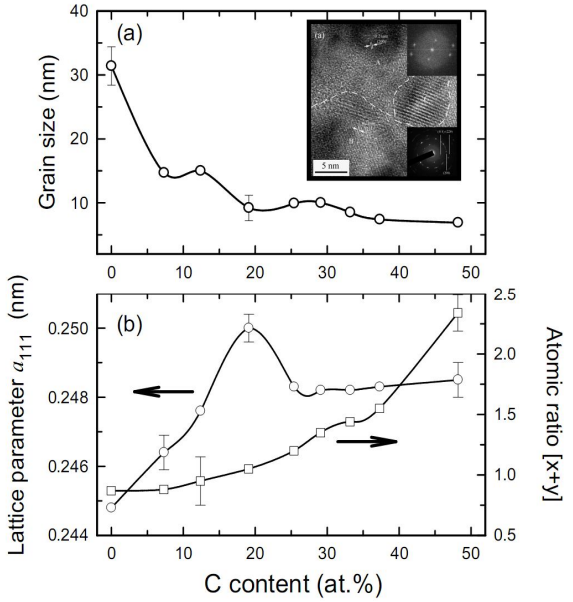

FIGURE 2. Dependence of the (a) grain size, (b) lattice parameter a_{111} and atomic ratio (x+y) in TiC_xN_y thin films as a function of C content. The inset of (a) shows the HRTEM image obtained from a C-free pure TiN film.

Figure 2(b) shows the dependence of atomic ratio[x+y] and lattice parameter a (calculated from XRD (111) diffraction peaks) on C content. Obviously, by addition of C into a growing TiN film, two main nanostructures have been observed: (i) SS Ti(N,C) in the case of atomic ratio (x+y) less than one unit; (ii) two-phase nanocomposite nc-Ti(N,C)/a-(C,CN_x) in the case of atomic ratio (x+y) more than one unit. When the atomic ratio (x+y) is close to one unit a nanostructure transition from SS to nanocomposite structure took place, which is further proved by the change in lattice space of nanocrystallites with C content. Figure 2(b) also shows that the lattice space linearly increases from 0.245 nm of pure TiN to 0.248 nm of $TiC_{0.24}N_{0.71}$ (~12.4 at.% C), and further to 0.25nm of $TiC_{0.39}N_{0.66}$ (19.1 at.%, at this C content the atomic ratio is 5% more than one unit). They are consistent with the corresponding measured values in the HRTEM images. However, when the C content is further increased to more than ~25.4 at.% (corresponding to atomic ratio of 1.20) a reduced lattice space with an almost constant value ~0.248 nm is found.

The MC simulated microstructures (not shown here) under different amorphous volume fraction (V_a) are in good agreement with those measured by HRTEM. The grain growth evolutions show that with increasing V_a, the transformation from nc/nc grain boundary (GB)-curvature-driven growth to a/nc GB-curvature-driven growth has been found. In the case of grains incompletely enclosed by amorphous phases, the general state of grain i is: one part of its GB is the a-/n- GB and the other part is the n-/n- GB. n_{AB}^i and n_{AA}^i indicate the number of lattice sites in a-/n- GB and n-/n- GB of grain i, respectively. For grain i, its a-/n- interfacial energy E_{AB}^i and n-/n- GB energy E_{AA}^i are $E_{AB}^i = n_{AB}^i J_{AB}$ and $E_{AA}^i = n_{AA}^i J_{AA}$. The mean energy exerted on a-/n- boundaries and n-/n- boundaries per grain can be calculated as $\langle E_{AB}\rangle = \sum_{i=1}^{m} E_{AB}^i / m$ and $\langle E_{AA}\rangle = \sum_{i=1}^{m} E_{AA}^i / m$.

Figure 3 displays the dependence of calculated parameters $\langle E_{AB}\rangle$, $\langle E_{AA}\rangle$ and $|\Delta E|$ on V_a after 1500 MC steps. Three characteristic regimes (I, II and III) can be divided according to the values of $\langle E_{AB}\rangle$ and $\langle E_{AA}\rangle$. In regime I, $\langle E_{AA}\rangle$ is larger than $\langle E_{AB}\rangle$ and $|\Delta E|$ decreases to zero with increasing V_a up to 23%, indicating that a dramatic driving force exerts on n-/n- boundaries at lower V_a, which drags n-/n- boundaries to slide and leads to entirely the n-/n- GB-curvature-driven growth realized by site re-orientation between crystal species. The grains with few amorphous species on its GB and larger sizes have stronger driving force and can grow more rapidly than those with average sizes. Therefore, great inhomogeneous growth among grains in this two-phase system will be expected, which is significantly different from the GB-curvature-driven growth in a single-phase system.

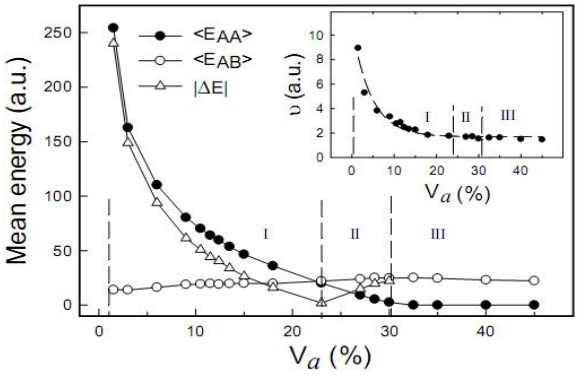

FIGURE 3. Dependence of $<E_{AA}>$, $<E_{AB}>$, and $|\Delta E|$ on V_a after 1500 MC steps. Three regimes are divided by vertical dashed lines. Inset is the grain growth rate υ as a function of V_a in the grain growth duration from 500 to 1500 MC steps.

In regime II, $|\Delta E|$ increases from zero to a constant with increasing V_a up to 30% and $<E_{AB}>$ becomes larger than $<E_{AA}>$, which drives a-/n- boundaries to glide. For a-/n- boundaries, their sliding acquires two steps as site exchange between crystal and amorphous species first and then re-orientation. Therefore, the sliding velocity should be slower than that of n-/n- boundaries. For the higher V_a in regime II, the grain growth is dominantly controlled by the a-/n- GB-curvature-driven growth and more homogenous growth process than that in regime I is expected. In regime III with V_a >30%, there is no $|\Delta E|$ i.e. no driving force exerted on a-/n- boundaries because the energy in every site of the boundary is J_{AB}. Species B prefers to adhere to grains and separates two species A with different orientations by site exchanges because J_{AA} is larger than J_{AB}. Also, species A in smaller grains undergoes numerous site exchanges and finally arrives at large grain boundaries, and then takes re-orientation to reduce the energy from J_{AA}. It is shown that site exchange dominantly decides the grain growth, which can be considered as a diffusion process of two kinds of species driven by the difference between J_{AA} and J_{AB}. This growth mode is called as diffusion-controlled growth, in which the constant sliding velocity of a-/n- boundaries is obtained under a given temperature in the simulation.

CONCLUSION

In summary, there are three indications, which are related to nanostructure behavior of nanocomposite nc-TiN/a-(C,CN_x) films. (i) In the case of SS Ti(N, C) incorporated C fully dissolved into lattice of TiN and expanded its lattice space, linearly increasing the lattice space with C content. (ii) In the case of two-phase nanocomposite thin films containing more than 25.4 at.% C, more incorporated C was preferential for formation of amorphous matrices rather than dissolution into nanocrystallites, and the dissolved amount of C in nanocrystallites was almost constant regardless of C content. (iii) It is interesting to note that this linear increase in lattice space extends to the highest value in this study in $TiC_{0.39}N_{0.66}$ (19.1 at.% C) where a nanocomposite thin film was just formed, revealing that more C dissolved into nanocrystallites in this film than those incorporating more C. One possible explanation is that an uncompleted spinodal phase segregation took place in $TiC_{0.39}N_{0.66}$ because few C precipitation did not provide enough the Gibbs free energy for phase segregation. More C hence remained in the lattice of supersaturated nanocrystallites, thus its lattice space linearly expanded to the greatest degree. When C content was more than 25.4 at%, more C precipitation provided a high the Gibbs free energy enough for full phase segregation, thus stoichiometric Ti(N,C) was formed along with amorphous matrices.

ACKNOWLEDGMENTS

This work was supported by the Research Grant Council of the Hong Kong Special Administrative Region, China [Project No. CityU 120611 (9041679)].

REFERENCES

[1] S. Veprek, J. Vac. Sci. Technol. A 17, 2401 (1999).
[2] J. Musil, Surf. Coat. Technol. 125, 322 (2000).
[3] D. Martínez-Martínez, J. C. Sánchez-Lopez, T. C. Rojas, A. Fernández, P. Eaton, and M. Belin, Thin Solid Films 472, 64 (2005).
[4] M. Stüber, H. Leiste, S. Ulrich and D.Schild, Surf. Coat. Technol. 150, 218 (2002).
[5] D.J. Srolovitz, J. Vac. Sci. Technol. A 4, 2925 (1986).
[6] D.J. Srolovitz, A. Mazor, and B.G. Bukiet, J. Vac. Sci. Technol. A 6, 2371 (1988).
[7] Z.J. Liu, C.H. Zhang, Y.G. Shen, and Y.W. Mai, J. Appl. Phys. 95, 758 (2004).
[8] C.G. Granqvist and R.A. Buhrman, J. Appl. Phys. 47, 2200 (1976).
[9] C. A. Carrasco, V. Vergara S., R. Benavente G., N. Mingolo, J. C. Rios, Mater. Character. 48, 81 (2002).

★★★